Received: 19 February 2020

DOI: 10.1002/mma.6457

SPECIAL ISSUE PAPER

WILEY

Analytical solution of free convection heat transfer of hybrid nanofluids over a vertical flat plate embedded in a porous medium

Mehdi Ghalambaz[1,2] | **Aminreza Noghrehabadi**[3] | **Ali Chamkha**[4] | **Sohail Nadeem**[5,6]

[1]Institute of Research and Development, Duy Tan University, Da Nang, 550000, Vietnam

[2]Faculty of Electrical – Electronic Engineering, Duy Tan University, Da Nang, 550000, Vietnam

[3]Department of Mechanical Engineering, Shahid Chamran University of Ahvaz, Ahvaz, Iran

[4]Mechanical Engineering Department, Prince Mohammad Endowment for Nanoscience and Technology, Prince Mohammad Bin Fahd University, Al-Khobar, Saudi Arabia

[5]Mathematics and Its Applications in Life Sciences Research Group, Ton Duc Thang University, Ho Chi Minh City, Vietnam

[6]Faculty of Mathematics and Statistics, Ton Duc Thang University, Ho Chi Minh City, Vietnam

Correspondence
Sohail Nadeem, Ton Duc Thang University, Ho Chi Minh City, Vietnam.
Email: sohail.nadeem@tdtu.edu.vn

The natural convection heat transfer of hybrid nanofluids over a vertical plate embedded in a saturated Darcy porous medium is analytically investigated. The base partial differential equations were reduced to a set of high-order nonlinear differential equations by using appropriate similarity variables. A new analytical solution based on the power series–transformation method is presented, and the effect of the presence of hybrid nanoparticles in the form of nondimensional parameters is investigated.

KEYWORDS

hybrid nanofluids, porous media, symbolic power series, transformation method

1 | INTRODUCTION

Nanofluids are engineered fluids containing nanoscale-sized nanoparticles dispersed in a conventional heat transfer liquid. The nanofluids are known with thermally enhanced thermo-physical properties.[1–3] Because of the enhanced heat transfer performance, nanofluids are proposed as good potential candidates to utilize in many engineering sectors such as heat exchangers,[4] cooling of computer and electronic devises,[5] thermal energy storages,[6] the coolant in machining, and engine cooling of vehicles.[7]

The natural convection in porous media includes crucial applications in a number of technological and engineering processes such as crude oil extraction, filtration, transpiration cooling, and storage of radioactive nuclear waste materials.[8] A vertical surface covered with conductive fins, the walls of an atomic west container buried in the soil, and the walls covered with packed beds are just simple examples of plates embedded in porous media.

There are many numerical and analytical approaches that have been utilized to study the free convection heat transfer over vertical plate embedded in a porous medium. Cheng and Minkowycz[9] examined the free convection

of a regular fluid about a vertical flat plate embedded in a saturated porous medium. They[9] assumed a proscribed temperature for the surface of the plate, which can be varied with the distance from the origin. The authors transformed the partial differential equations, governing the heat and momentum of the fluid, into a set of nonlinear ordinary differential equations (ODEs) by the aid of the similarity variables. Later, the deduced ODE is solved using the Rong–Kutta method. Following, Cheng and Minkowycz,[9] Belhachmi et al.[10] solved the nonlinear ODEs governing the equations of Cheng and Minkowycz[9] using the finite difference method associated with the shooting technique. Following the study of Cheng and Minkowycz,[9] different aspects of boundary layer flow and heat transfer over a flat plate embedded in porous media including thermophoresis,[11] radiation,[12] internal heat generation,[13] non-Newtonian effects,[14] magnetic[15] and chemical reaction,[16,17] and phase change[18] effects have been numerically analyzed.

Xu[19] solved the nonlinear ODEs of Cheng and Minkowycz[9] utilizing the homotopy analysis method (HAM). The HAM is a powerful method to deal with nonlinear problems; however, this method needs too many terms to obtain a sufficiently accurate solution. Hence, it required laborious and time-consuming manipulations, and in most cases, it needs symbolic computer procedures. Chamkha and Quadri[20] have numerically studied the boundary layer flow and heat transfer of a binary mixture fluid in porous media using an implicit finite-difference method.

Effective cooling techniques are extremely required for removing heat from any high-energy device. The thermal conductivity of the common heat transfer liquids such as ethylene glycol, engine oil, and water is low in comparison with the thermal conductivity of the solids. Thus, dispersing very fine solid particles in the scale of few nanometers can enhance the thermal conductivity of the conventional heat transfer liquids. As mentioned, a nanofluid is the suspension of solid nanoparticles dispersed in a base fluid.[21] Different shapes, sizes, and types of nanoparticles have been utilized to synthesis nanofluids.[1,2] Thus, the thermo-physical properties of nanofluids are a function of the volume fraction, size, shape, and the constricting materials of nanoparticles.[1–3] The thermo-physical properties of nanofluids can be measured directly by experimental tests.[22] In addition, several models can evaluate the thermo-physical properties of nanofluids.[23–26]

Hybrid nanofluids are a new type of nanofluids that benefit from the advantage of two kinds of nanoparticles. Mehryan et al.[27] numerically investigated the flow and heat transfer of hybrid nanofluids in a porous enclosure. The results showed that the presence of hybrid nanoparticles could enhance the natural convection heat transfer in some circumstances where the interaction between the porous matrix and the nanofluid inside the pores is weak. Ghalambaz et al.[28] numerically addressed the free convection heat transfer of Ag–MgO hybrid nanofluids in a porous enclosure. They concluded that the presence of hybrid nanoparticles could reduce the free convection heat transfer in certain circumstances. The free convection heat transfer of hybrid nanofluids has also be investigated in cavities with no porous medium in various shapes such as an L-shaped cavity,[29] a semicircular cavity,[30] a partitioned cavity,[31] and a cylinder cavity.[32] The nanoencapsulated phase change materials are another type of hybrid nanofluid, investigated in some of the recent researches.[18,33–35]

In the convective heat transfer application of nanofluids, the overall heat transfer enhancement is the result of the simultaneous variation of the thermophysical properties. For instance, the presence of nanoparticles in the base fluid increases the thermal conductivity and dynamic viscosity of the nanofluids. The increase of the thermal conductivity tends to increase the natural convection heat transfer coefficient; in contrast, the increase of the dynamic viscosity of the nanofluid tends to decrease the natural convection heat transfer coefficient. Thus, the convective heat transfer analysis of nanofluids is crucial in the selection of the appropriate types of nanofluids in the engineering heat transfer applications. Indeed, the presence of an analytical solution can effectively facilitate the selection of the sufficient type of nanoparticles to increase the heat transfer rate. In addition, the presence of a compact analytical solution leads to a better understanding of the nonlinear nature of the system.

The present study aims to analytically study the natural convection heat transfer of hybrid nanofluids over a flat plate embedded in a saturated porous medium. The analytical solution is obtained using a combination of symbolic power series solution, Padé approximants, and a transformation approach. The obtained analytical solution is also valid for common pure fluids.

2 | MATHEMATICAL FORMULATION

Consider a vertical flat plate embedded in a porous medium with a porosity of ε and permeability of κ. The porous medium is saturated with a homogenous hybrid nanofluid. The plate is hot, and hence, the fluid in the vicinity of the

plate gets hot. The hot fluid expands and tends to move upward; the cold fluid tends to replace the hot fluid. Hence, there is a buoyancy-driven flow over the plate. The coordinate system is chosen such that y is perpendicular to the plate into the porous space and x is aligned with the plate and opposite to the gravity acceleration. The plate is subject to a prescribed temperature T_w, which varies with distance to the origin as $T_w = T_\infty + Ax^\lambda$ where λ and A are two arbitrary constants. The term $\lambda = 0$ leads to the case of the isothermal plate, whereas $\lambda = 1/3$ yields the case of plate subject to a constant heat flux.[36] The volume fractions of the nanoparticles are ϕ_1 *and* ϕ_2. The hybrid nanofluid far from the plate is quiescent and is at a constant temperature of T_∞. A schematic view of the physical model and coordinate system is depicted in Figure 1.

Considering the common boundary layer approximations and the Boussinesq approximation, the governing equations of continuity, momentum, and thermal energy for hybrid nanofluids over a flat plate are written as[36]

$$\frac{\partial u}{\partial x} + \frac{\partial v}{\partial y} = 0, \tag{1}$$

$$u = -\frac{\kappa}{\mu_{hnf}}\left(\frac{\partial p}{\partial x} - \rho_{hnf} g \beta_{hnf}(T - T_\infty)\right), \tag{2a}$$

$$\frac{\partial p}{\partial y} = 0, \tag{2b}$$

$$u\frac{\partial T}{\partial x} + v\frac{\partial T}{\partial y} = \alpha_{hnf,eff}\frac{\partial^2 T}{\partial y^2}. \tag{3}$$

Based on the problem description, the boundary conditions at the plate are

$$y = 0: \quad v = 0, \ T = T_\infty + Ax^\lambda, \ x \geq 0,$$

and the boundary conditions far from the plate are

$$y \to \infty: \ u = 0, \ T = T_\infty. \tag{4}$$

In the above equations, u denotes the Darcy's velocity along the plate and v denotes the Darcy's velocity component of the flow perpendicular to the plate (along the y direction).

T and P denote the temperature and the pressure of the hybrid nanofluid, respectively. The quantities of β_{hnf}, ρ_{hnf}, and μ_{hnf} are the thermal volume expansion coefficient, the density, and the dynamic viscosity of the hybrid nanofluid, respectively. Here, g is the gravity acceleration, and κ is the permeability of the porous medium. The symbol $\alpha_{hnf,eff}$ represents the effective diffusivity of the hybrid nanofluid and porous space. The effective diffusivity of the hybrid nanofluid is the ratio of the effective thermal conductivity of the hybrid nanofluid to the thermal capacity of the hybrid nanofluid as $\alpha_{hnf,eff} = k_{hnf,eff}/(\rho_{hnf} \times Cp_{hnf})$, where $k_{hnf,eff}$ is the effective thermal conductivity of the hybrid nanofluid and Cp_{hnf} is the specific thermal capacity of the hybrid nanofluid.

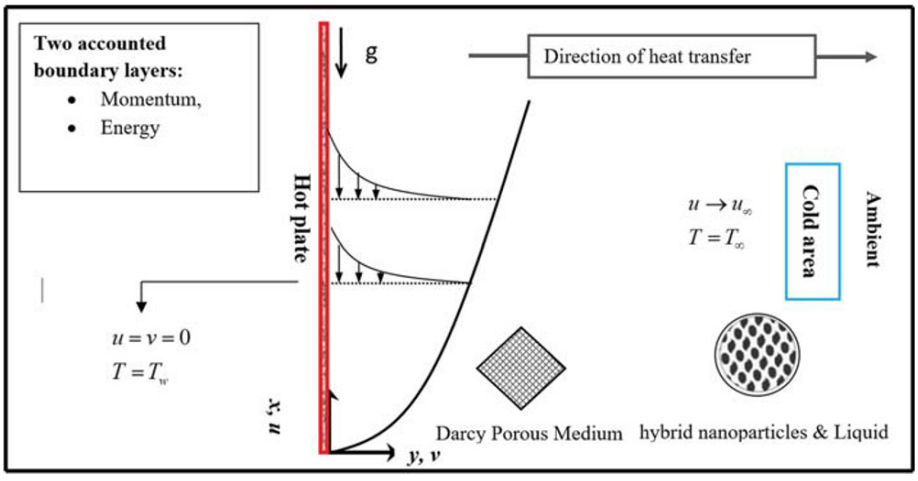

FIGURE 1 Schematic view of the plate and mathematical models [Colour figure can be viewed at wileyonlinelibrary.com]

The thermophysical properties of the hybrid nanofluid can be directly measured from the experimental test or evaluated using the thermo-physical models. An excellent review of the thermophysical properties of hybrid nanofluids can be found in Babu et al.[26] and Sundar et al.[37] Some general relations for the thermophysical properties of hybrid nanofluids are summarized in Table 1, where the subscripts 1, 2, and f denote the first type nanoparticles, the second type nanoparticles, and the base fluid, respectively.

Moreover, the thermophysical properties can be computed by using the available experimental data and correlations. Following Sundar et al.[38] the thermophysical properties of MWCNT–Fe_3O_4/water are summarized in Table 2 for the working temperature of 40°C.

Now, the following stream function is introduced to satisfy the continuity equation 1:

$$u = \frac{\partial \psi}{\partial y}, \quad v = -\frac{\partial \psi}{\partial x}. \tag{5}$$

The pressure is eliminated from the momentum equations, that is, Equations 2a and 2b, by cross-differentiations and subtracting the resulting equations. Consider the following similarity variables:

$$\eta = \frac{y}{x} Ra_x^{\frac{1}{2}}, \ \theta = \frac{T - T_\infty}{T_w - T_\infty}, \ \psi = \left(\alpha_{eff}\right)_f f(\eta) Ra_x^{\frac{1}{2}} \tag{6}$$

and the Rayleigh–Darcy number as

$$Ra_x = \frac{g\beta_f \kappa \rho_f x (T_w - T_\infty)}{\mu_f \alpha_{eff,f}}. \tag{7}$$

Here, the similarity variables are introduced based on the base fluid thermo-physical properties. Hence, β_f, ρ_f, and μ_f denote the thermal volume expansion, the density, and the dynamic viscosity of the base fluid. $\alpha_{eff,f}$ represents the effective thermal conductivity of the base fluid, and the porous medium, introduced as $\alpha_{eff,f} = k_{eff,f}/(\rho_f.\ Cp_f)$ where $k_{eff,f}$ is the thermal conductivity of the base fluid, and Cp_f is the thermal capacity of the base fluid. Invoking the similarity

TABLE 1 Thermal properties of hybrid nanofluids Babu et al.[26]

Properties	Hybrid nanofluids
Density	$\rho_{hnf} = \phi_1\rho_1 + \phi_2\rho_2 + (1 - \phi_{hnf})(\rho Cp)_f$
Heat capacity	$(\rho Cp)_{hnf} = \phi_1(\rho Cp)_1 + \phi_2(\rho Cp)_2 + (1 - \phi_{hnf})(\rho Cp)_f$
Thermal expansion	$(\rho\beta_p)_{hnf} = \phi_1(\rho\beta)_1 + \phi_2(\rho\beta)_2 + (1 - \phi_{hnf})(\rho\beta)_f$
Dynamic viscosity	$\mu_{hnf} = \mu_f(1 - \phi_1 - \phi_2)^{-2.5}$
Thermal conductivity	$\frac{k_{hnf}}{k_f} = \left\{\frac{\phi_1 k_1 + \phi_2 k_2}{\phi_1 + \phi_2} + 2k_f + 2(\phi_1 k_1 + \phi_2 k_2) - 2(\phi_1 + \phi_2)k_f\right\} \times \left\{\frac{\phi_1 k_1 + \phi_2 k_2}{\phi_1 + \phi_2} + 2k_f - (\phi_1 k_1 + \phi_2 k_2) + (\phi_1 + \phi_2)k_f\right\}^{-1}$

TABLE 2 The thermophysical properties of MWCNT–Fe_3O_4/water and computed corresponding values of Nc and Nv at the working temperature of 40°C for glass ball porous matrix with the porosity of $\varepsilon = 0.5$

Thermophysical data from Sundar et al.[38]					Computed	
Volume fraction (%)	Density (kg/m^3)	Thermal conductivity (W/m K)	Viscosity (mPa·s)	Specific heat (J/kg K)	Na	Nv^a
φ = 0.0	992.0	0.631	0.54	4179	1	1
φ = 0.1	1002.34	0.72	0.61	4179.66	1.0419	1.1180
φ = 0.3	1009.56	0.7656	0.76	4180.99	1.0608	1.3829

[a]Due to a low concentration of nanoparticles $\beta_{nf}/\beta_f \sim 1$.

variables, that i, Equation 6, the partial differential equations of the momentum and energy are transformed to the following ODEs:

$$Nvf''(\eta) = \theta'(\eta), \tag{8}$$

$$Na\theta''(\eta) + \left(\frac{\lambda+1}{2}\right) f(\eta)\theta'(\eta) - \lambda f'(\eta)\theta(\eta) = 0. \tag{9}$$

The transformed boundary conditions are

$$f(0) = 0, \theta(0) = 1, \tag{10a}$$

$$f'(\infty) = 0, \theta(\infty) = 0, \tag{10b}$$

where Na is the number of thermal diffusivity and Nv is the number of viscosity as

$$Na = \frac{k_{hnf,eff}\rho_f Cp_f}{k_{f,eff\,f}\rho_{hnf} Cp_{hnf}}, Nv = \frac{\mu_{hnf}\rho_f\beta_f}{\mu_f\rho_{hnf}\beta_{hnf}}, \tag{11}$$

where the effective thermal conductivity of the porous medium and the fluid/nanofluid can be obtained as k_{eff} = (1-ε) k_f + ε k_m. Here, ε indicates the porosity of the porous medium, and k_m is the thermal conductivity of the porous medium. For a glass ball porous medium, the thermal conductivity (k_m) is 1.05 W/m K.[39]

Based on the energy balance at the plate, the heat transferred from the surface is equal to the heat transferred into the porous space and the hybrid nanofluid; hence, the energy balance at the surface is written as

$$q'' = -k_{eff,hnf}\left(\frac{\partial T}{\partial y}\right)_{y=0} = -k_{eff,hnf}A^{\frac{3}{2}}\left(\frac{\rho_f g\beta_f\kappa}{\mu_f\alpha_{eff\,f}}\right)^{\frac{1}{2}} x^{\frac{3\lambda-1}{2}}\theta'(0). \tag{12}$$

Equation 12 can be rewritten in a nondimensional from as

$$\frac{Nu_x}{Ra_x^{\frac{1}{2}}} = -\frac{k_{eff,hnf}}{k_{eff\,f}}\theta'(0), \tag{13}$$

where the local Nusselt number (Nu_x) is

$$Nu_x = \frac{hx}{k_{eff\,f}}, \tag{14}$$

where h is the convective heat transfer coefficient at the wall, which is defined by Newton's cooling law as $h = q''/(T_w\text{-}T_\infty)$.7

In Equation 13, $Nu_x/Ra_x^{1/2}$ is the reduced Nusselt number (Nur), which is the nondimensional heat transfer parameter over the plate. The reduced Nusselt number represents the heat transfer from the surface. This parameter is the main parameter of interest in practical applications of boundary layer heat transfer over the plate. It is worth noticing that substituting $\lambda = 1/3$ in Equation 12, the heat flux (q'') at the plate is independent of x, which represents the uniform heat flux at the surface. Thus, the special case of $\lambda = 1/3$ is the case of constant heat flux at the surface, which is of many practical applications. Equation 13 shows that the reduced Nusselt number (Nur) is a function of $\theta'(0)$, which should be evaluated from the solution of Equations 8 and 9 subject to the boundary conditions in Equations 10a and 10b. Finally, the total heat transfer rate through the plate of height L and unit of width is evaluated as

$$\bar{q}' = \int_0^L q''(x)dx = \left(k_{eff}\right)_{nf} A^{\frac{3}{2}} \left(\frac{g\beta_f K}{\upsilon_f \alpha_{m,f}}\right)^{\frac{1}{2}} \left(\frac{2}{1+3\lambda}\right) L^{\frac{(1+3\lambda)}{2}} [-\theta'(0)]. \tag{15}$$

3 | SOLUTION METHOD

3.1 | Symbolic power series

As there is not an independent variable (η) in Equation 8, it can easily be integrated as

$$Nvf'(\eta) = \theta(\eta) + C_0, \tag{16}$$

where invoking one of the boundary conditions of Equation 10b gets

$$Nvf'(\eta) = \theta(\eta). \tag{17}$$

Now, substituting the above equation into Equation 9 gives

$$Naf''' + \left(\frac{\lambda+1}{2}\right) f.f'' - \lambda.f'^2 = 0, \tag{18}$$

which is a third-order nonlinear boundary value differential equation. Using Equation 17, the boundary conditions are also obtained as

$$f(0) = 0, f'(0) = \frac{1}{Nv}, f'(\infty) = 0. \tag{19}$$

Here, the symbolic power series method, in Guzel and Bayram[40] and Celik and Bayram,[41] is utilized to solve the governing equation of hybrid nanofluid over the plate (Equation 18), subject to its transformed boundary conditions, Equation 19. The basic idea of symbolic power series is explained in Celik and Bayram.[41] Following Celik and Bayram,[41] Equation 18 and the corresponding boundary conditions (Equation 19) are rewritten in a more convenient form as

$$df_1 = f_2,\ df_2 = f_3\ ,\ df_3 = \frac{\lambda\, {f_2}^2 - \left(\frac{\lambda+1}{2}\right) f_1 f_3}{Na}, \tag{20}$$

$$f_1(0) = 0, f_2(0) = 1/Nv, f_3(0) = K, \tag{21}$$

where K is an unknown constant, which can be determined later.

Based on the symbolic power series method, the values of f_1, f_2, and f_3 are needed at the starting point. Hence, starting with $\eta = 0$, the values of f_1 and f_2 are 0 and $1/Nv$, respectively. However, the value of f_3 is unknown at this starting point. In this case, the unknown value of f_3 at $\eta = 0$ is replaced by $f_3 = K$, where K is an unknown constant, which later can be evaluated using the remaining unused boundary condition, that is, $f_2(\infty) = 0$.

Based on the symbolic power series method, and starting from $\eta = 0$, the power series solution of Equation 20 is written as

$$\begin{aligned} f_1 &= 0 + e_{11}\eta \\ f_2 &= \frac{1}{Nv} + e_{12}\eta \\ f_3 &= K + e_{13}\eta, \end{aligned} \tag{22}$$

where e_{1i} and $i = 1 \ldots 3$ are the unknowns, which form the first-order series of the solution. Now, substituting Equation 22 into Equation 20, and discarding the higher order terms (of η), results in the following algebraic equation:

$$\begin{aligned} &e_{11} - \frac{1}{Nv} - e_{12}\eta = 0 \\ &e_{12} - K - e_{13}\eta = 0 \\ &e_{13} - \frac{1}{a}\lambda\left(e_2\eta + \frac{1}{z}\right)^2 - e_{11}\eta\left(\frac{\lambda}{2} + \frac{1}{2}\right)(K + e_{13}\eta) = 0. \end{aligned} \tag{23}$$

Solving the above algebraic equations for e_{1i} gives

$$\begin{aligned} e_{11} &= \frac{1}{Nv} \\ e_{12} &= K \\ e_{13} &= \frac{\lambda}{NaNv^2}. \end{aligned} \tag{24}$$

The evaluated values of e_{1i} are substituted in Equation 22 to form the first-order series of the solution. Now, taking into account the second-order approximation of the solution gives

$$\begin{aligned} f_1 &= \frac{\eta}{Nv} + e_{11}\eta^2 \\ f_2 &= \frac{1}{Nv} + K\eta + e_{12}\eta^2 \\ f_3 &= K + \frac{\lambda}{NaNv^2}\eta + e_{13}\eta^2. \end{aligned} \tag{25}$$

Invoking Equation 25 and substituting into Equation 20 and again discarding the higher-order terms (of η) result in the following algebraic equation for e_{2i} and $i = 1 \ldots 3$ gives

$$\begin{aligned} e_{21} &= \frac{K}{2} \\ e_{22} &= \frac{\lambda}{2NaNv^2} \\ e_{23} &= \frac{3K\lambda - K}{4NaNv}. \end{aligned} \tag{26}$$

Again, substituting the evaluated values of e_{2i} into Equation 25 and taking into account a higher term of η give a higher-order series solution. Following this procedure, the power series solution of f_1 is obtained after 11 iterations:

$$\begin{aligned} f_1(\eta) = {} & \frac{\eta}{Nv} + \frac{K\eta^2}{2} + \frac{\lambda}{6NaNv^2}\eta^3 - \frac{K(1-3\lambda)}{48NaNv}\eta^4 - \frac{\left(NaK^2Nv^3 - 3NaK^2\lambda Nv^3 - 2\lambda^2 + 2\lambda\right)}{240Na^2Nv^3}\eta^5 + \frac{\left(19K\lambda^2 - 18K\lambda + 3K\right)}{(2880Na^2Nv^2)}\eta^6 \\ & + \frac{\begin{pmatrix} 11K^2Nv^3Na - 42\lambda K^2Nv^3Na \\ + 27K^2Nv^3Na\lambda^2 - 16\lambda^2 + 16\lambda^3 + 8\lambda \end{pmatrix}}{20160Nv^4Na^3}\eta^7 + \frac{K\begin{pmatrix} 161\lambda - 297\lambda^2 + 167\lambda^3 - 84\lambda K^2Nv^3Na \\ + 54\lambda^2K^2Nv^3Na + 22K^2Nv^3Na - 15 \end{pmatrix}}{322560Nv^3Na^3}\eta^8 \\ & + \frac{\begin{pmatrix} 709\lambda K^2Nv^3Na - 1035K^2Nv^3Na\lambda^2 - 129K^2Nv^3Na \\ + 527\lambda^3K^2Nv^3Na - 304\lambda^3 + 104\lambda^4 + 184\lambda^2 - 48\lambda \end{pmatrix}}{2903040Nv^5Na^4}\eta^9 \\ & + \frac{K\begin{pmatrix} -1910\lambda + 3342\lambda K^2Nv^3Na - 750K^2Nv^3Na - 3834K^2Nv^3Na\lambda^2 \\ + 5392\lambda^2 - 6298\lambda^3 + 2295\lambda^4 + 1674\lambda^3K^2Nv^3Na + 105 \end{pmatrix}}{58060800Nv^4Na^4}\eta^{10}. \end{aligned} \tag{27}$$

Usually, the convergence range of power series is small. However, converting the series solution into a ratio series form using the Padé approximants may significantly increase the convergence range of solutions.[42,43] Following the Padé method,[42,43] the Padé series with the size of (2, 2) of Equation 27 is evaluated as

$$f_1(\eta)=\frac{1}{48}\frac{[(3456K^2Na^2Nv^3-2304\lambda Na)\eta+(1728K^3Na^2Nv^4-1440NvNaK\lambda-288KNvNa)\eta^2]}{\left[72K^2Na^2Nv^4-48NvNa\lambda-6KNv^2Na(1+\lambda)\eta+\left(-9\lambda K^2Nv^3Na+3K^2Nv^3Na+8\lambda^2\right)\eta^2\right]}. \tag{28}$$

For instance, in the case of an isothermal flat plate, that is, $\lambda=0$, the Padé (4, 4) of Equation 27 is evaluated as

$$f_1(\eta)=\frac{\left(\begin{array}{l}(486091368000Nv^7Na^4K^4-61725888000K^2Na^3Nv^4-65840947200NvNa^2)\eta\\+\left(243045684000Nv^8Na^4K^5-208324872000Nv^5Na^3K^3+41150592000Nv^2Na^2K\right)\eta^2\\+\left(-3857868000Nv^6Na^3K^4+15382483200K^2Na^2Nv^3-6009292800Na\right)\eta^3\\+(28934010000Nv^7Na^3K^5-24200467200Nv^4Na^2K^3+4964198400KNvNa)\eta^4\end{array}\right)}{136080\left(\begin{array}{l}3572100Nv^8Na^4K^4-453600Nv^5Na^3K^2-483840Nv^2Na^2\\+\left(-1304100Nv^6Na^3K^3+544320Nv^3Na^2K\right)\eta\\+(425250Nv^7Na^3K^4-133920Nv^4Na^2K^2-17280NvNa)\eta^2\\+(-38430Nv^5Na^2K^3+14880Nv^2NaK)\eta^3\\+\left(2205K^4Nv^6Na^2-840K^2Nv^3Na+64\right)\eta^4\end{array}\right)}. \tag{29}$$

It is worth noticing that the parameter of K is unknown yet in Equations 28 and 29. In order to achieve a full analytical solution for the problem, the undetermined value of K is required to be determined by utilizing the remaining unused boundary condition of $f_2(\infty)\to 0$. However, the direct use of this boundary condition is not possible because the accuracy of the series solution significantly reduces as $\eta\to\infty$. Furthermore, the appropriate physical value of the infinity is not clear. Utilizing a small asymptotic value ∞ leads to physical error, and utilizing a large asymptotic value leads to divergence of the solution and invalid values of K. Thus, the direct implementation of the asymptotic boundary condition $f_2(\infty)\to 0$ is not practical at this stage. Here, the treatment of the next section is utilized to facilitate the evaluation of K without assuming an asymptotic boundary condition.

3.2 | The transformed differential equation

Let us assume the following changes of variables:

$$X=f_2(\eta), \tag{30}$$

$$Y(X)=f_3(\eta). \tag{31}$$

It is clear that $f_3(\eta)=\mathrm{d}f_2(\eta)/\mathrm{d}\eta$; and hence, using Equations 30 and 31, $Y(X)$ is written as

$$Y=\frac{df_2(\eta)}{d\eta}=\frac{dX}{d\eta}, \tag{32}$$

$$Y'=\frac{dY}{dX}=\frac{df_3}{f_3}, \tag{33}$$

$$Y''=\frac{d^2Y}{dX^2}=\frac{dY'}{dX}=\frac{d^2f_3\times f_3-(df_3)^2}{f_3^2}. \tag{34}$$

On the other hand, Equations 18 can be rewritten as

$$f_1 = \frac{2\left(\lambda f_2^2 - Na d f_3\right)}{(\lambda+1) f_3}. \tag{35}$$

By invoking Equations 30–33, the above equation is written as

$$f_1 = \frac{2(\lambda X^2 - Na Y Y')}{(\lambda+1) Y}. \tag{36}$$

Applying the notation of Equation 20, Equation 18 can be rewritten as

$$Na d f_3 + \left(\frac{\lambda+1}{2}\right) f_1 f_3 - \lambda f_2^2 = 0. \tag{37}$$

Now, differentiating both sides of Equation 37 with respect to the dependent variable of η gives

$$\frac{d}{d\eta}\left(Na d(f_3) + \left(\frac{\lambda+1}{2}\right) f_1 f_3 - \lambda f_2^2\right) = Na d^2(f_3) + \left(\frac{\lambda+1}{2}\right)(f_3 f_2 + d(f_3) f_1) - 2\lambda f_3 f_2 = 0. \tag{38}$$

Substituting Equation 36 into Equation 38 results

$$Na d^2(f_3) + \left(\frac{\lambda+1}{2}\right)\left(f_3 f_2 + d(f_3)\left(\frac{2\left(\lambda f_2^2 - Na d(f_3)\right)}{(\lambda+1) f_3}\right)\right) - 2\lambda f_3 f_2 = 0. \tag{39}$$

Finally, the following transform equation is achieved by substituting Equations 30–34 into Equation 39:

$$Na Y'' Y^2 + XY\frac{1-3\lambda}{2} + \lambda . X^2 Y' = 0. \tag{40}$$

Now, the boundary condition should also represent in the form of new variables. The second boundary condition of Equation 21 indicates

$$X = f'(\eta) = \frac{1}{Nv}. \tag{41}$$

Substituting the first boundary condition Equation 21 into Equation 36 yields

$$\frac{\frac{2\lambda}{Nv^2}}{(\lambda+1) Y_{(1/Nv)}} - \frac{2Na Y'_{1/Nv}}{(\lambda+1)} = 0. \tag{42}$$

According to assumption equations (Equations 30 and 31), $Y(f'(\eta))=f''(\eta)$, as $\eta=0$ results $Y(f'(0))=f''(0)$ now assuming $f''(\eta)=K$ and using Equation 41 one can find that

$$Y_{(1/Nv)} = K. \tag{43}$$

Thus, as $\eta = 0$, Equation 36 yields

$$Y'_{(1/Nv)} = \frac{\lambda}{Nv^2 NaK}. \tag{44}$$

According to assumption equations (Equations 30 and 31) and boundary condition equation Equation 21, it is clear that $0 < x < 1/N$. Therefore, considering that as $\eta \to \infty$ results in $x \to 0$ and $f'(\infty) = f''(\infty) = 0$ and using Equation 31, it is clear that

$$f''(\infty) = Y(0) = 0. \tag{45}$$

Now, the second-order boundary value differential equation of Equation 40 subject to the boundary conditions of Equations 43–45 can be solved to obtain the undetermined value of K. It is worth mentioning that the differential Equation 40 is free of any asymptotic boundary condition. It should be noticed that the differential equation of Equation 40 is a second-order differential equation, and in Equations 43–45, there are three corresponding boundary conditions and an undetermined value of K. Thus, the solution of Equation 40 subject to the boundary conditions of Equations 43–45 would give the undetermined value of K.

Here, the symbolic power series is applied to solve the present boundary value differential equation. Attention to boundary conditions indicates that two of the boundary conditions of Equation 40 are proposed at the point $(1/Nv)$; hence, X is changed to $X + 1/Nv$ for convenience. Invoking the change of the variables, the differential equation of Equation 40 and the corresponding boundary conditions (Equations 43–45) are written as

$$NaY''Y^2 + \frac{1-3\lambda}{2}(X + 1/Nv)Y + \lambda.(X + 1/Nv)^2 Y' = 0, \tag{46}$$

$$Y_{(0)} = K, Y'_{(0)} = \frac{\lambda}{Nv^2 NaK}, Y_{(-1/Nv)} = 0. \tag{47}$$

Following the symbolic power series method, the second-order nonlinear differential equation of Equation 46 is written as a set of two first orders nonlinear differential equations as

$$dY_1 = Y_2, dY_2 = -\frac{\left((X + 1/Nv)Y_1 \frac{1-3\lambda}{2} + \lambda.(X + 1/Nv)^2 Y_2\right)}{NaY_1{}^2} \tag{48}$$

Subject to:

$$\begin{aligned} Y_1(0) &= K \\ Y_2(0) &= \frac{\lambda}{Nv^2 NaK} \end{aligned} \tag{49}$$

The first-order approximation of the series solution at $X = 0$ is written as

$$\begin{aligned} Y_1 &= K + e_{11}X \\ Y_2 &= \frac{\lambda}{Nv^2 NaK} + e_{12}X. \end{aligned} \tag{50}$$

Now, inserting Equation 50 into Equation 48, and discarding the higher-order terms (of X) results in the following algebraic equation for e_{1i}, $i = 1, 2$:

$$\begin{aligned} & e_{11} - e_{12}X - \frac{\lambda}{Nv^2 NaK} = 0, \\ & e_{12} + \frac{\lambda\left(e_{12}\eta + \frac{\lambda}{KNv^2 Na}\right)\left(\eta + \frac{1}{Nv}\right)^2 - \left(\frac{3\lambda}{2} - \frac{1}{2}\right)\left(\eta + \frac{1}{Nv}\right)(K + e_{11}\eta)}{Na(K + e_{11}\eta)^2}, \end{aligned} \tag{51}$$

which solving the above equation of e_{1i} gives

$$e_{11} = \frac{\lambda}{KNv^2Na}$$
$$e_{12} = \frac{\left(3NaK^2\lambda Nv^3 - NaK^2Nv^3 - 2\lambda^2\right)}{2K^3Nv^4Na^2}. \tag{52}$$

Substituting the obtained values of e_{1i} into Equation 50 and adding a higher-order term yield

$$Y_1 = K + \frac{\lambda\eta}{KNv^2Na} + e_{21}\eta^2,$$
$$Y_2 = \frac{\lambda}{KNv^2Na} - \frac{\eta\left(NaK^2Nv^3 - 3NaK^2\lambda Nv^3 + 2\lambda^2\right)}{2K^3Nv^4Na^2} + e_{22}\eta^2. \tag{53}$$

Again, substituting Equation 53 into Equation 48 and discarding the higher-order terms of X then solving for e_{2i}, $i = 1,2$, give

$$e_{21} = -\frac{\left(NaK^2Nv^3 - 3NaK^2\lambda Nv^3 + 2\lambda^2\right)}{4K^3Nv^4Na^2},$$
$$e_{22} = \frac{\left(3Na^2\lambda K^4Nv^6 - Na^2K^4Nv^6 - 10\lambda^2K^2Nv^3Na + 2\lambda K^2Nv^3Na + 6\lambda^3\right)}{4K^5Nv^6Na^3}. \tag{54}$$

Repeating the above procedure, the power series for Y_1 after four iterations is accomplished as

$$\begin{aligned} Y_1 = K &+ \frac{\lambda}{Nv^2NaK}X + \frac{1}{4}\frac{\left(3K^2Nv^3Na\lambda - K^2Nv^3Na - 2\lambda^2\right)}{Nv^4Na^2K^3}X^2 \\ &+ \frac{1}{12}\frac{1}{Nv^6Na^3K^5}\begin{pmatrix} 2K^2Nv^3Na\lambda - 10\lambda^2Nv^3NaK^2 \\ + 6\lambda^3 - K^4Nv^6Na^2 + 3K^4Nv^6Na^2\lambda \end{pmatrix}X^3 \\ &- \frac{1}{96}\frac{1}{Nv^8Na^4K^7}\begin{pmatrix} K^4Nv^6Na^2 - 20K^4Nv^6Na^2\lambda + 22K^2Nv^3Na\lambda^2 \\ + 59K^4Nv^6Na^2\lambda^2 - 122\lambda^3K^2Nv^3Na + 60\lambda^4 \end{pmatrix}X^4, \end{aligned} \tag{55}$$

where the above equation can be transformed into a Padé series of (2, 2) to attain an increased accuracy and convergence. Later, the undetermined value of K can be evaluated by invoking the remaining unused boundary condition in Equation 47, that is, $y_{(-1/Nv)} = 0$. Thus, converting the power series of Equation 55 into a Padé series of (2, 2) and substituting $-1/Nv$ in the deduced Padé series give the following equation:

$$\frac{648K\begin{pmatrix} Nv^{12}Na^4\left(\lambda - \frac{1}{3}\right)\left(\lambda - \frac{13}{27}\right)K^8 - \frac{35}{72}Nv^9Na^3\left(\frac{1}{15} - \frac{43}{315}\lambda - \frac{65}{63}\lambda^2 + \lambda^3\right)K^6 \\ -\frac{313}{162}Nv^6Na^2\lambda^2\left(\lambda^2 + \frac{16}{313} - \frac{55}{313}\lambda\right)K^4 + \frac{55}{27}Nv^3Na\lambda^4\left(\lambda - \frac{1}{11}\right)K^2 - \frac{5}{9}\lambda^6 \end{pmatrix}}{\begin{pmatrix} 648Nv^{12}Na^4\left(\lambda - \frac{1}{3}\right)\left(\lambda - \frac{13}{27}\right)K^8 - 9Nv^9Na^3\left(\frac{1}{3} - \frac{1}{9}\lambda - \frac{187}{9}\lambda^2 + \lambda^3\right)K^6 \\ -1204Nv^6Na^2\lambda^2\left(\lambda^2 + \frac{10}{301} - \frac{73}{301}\lambda\right)K^4 + 744Nv^3Na\left(\lambda - \frac{5}{31}\right)\lambda^4K^2 - 72\lambda^6 \end{pmatrix}} = 0. \tag{56}$$

If the above equation is equal to zero, its numerator should be zero; hence,

$$\begin{pmatrix} Nv^{12}Na^4\left(\lambda - \frac{1}{3}\right)\left(\lambda - \frac{13}{27}\right)K^8 - \frac{35}{72}Nv^9Na^3\left(\frac{1}{15} - \frac{43}{315}\lambda - \frac{65}{63}\lambda^2 + \lambda^3\right)K^6 \\ -\frac{313}{162}Nv^6Na^2\lambda^2\left(\lambda^2 + \frac{16}{313} - \frac{55}{313}\lambda\right)K^4 + \frac{55}{27}Nv^3Na\lambda^4\left(\lambda - \frac{1}{11}\right)K^2 - \frac{5}{9}\lambda^6 \end{pmatrix} = 0, \tag{57}$$

which solving for K^2 gives

$$K^2=\frac{1}{NaNv^3}Rotts\left(\begin{array}{l}\left(648\lambda^2-528\lambda+104\right)r^4+\left(325\lambda^2-21+43\lambda-315\lambda^3\right)r^3\\+\left(-1252\lambda^4+220\lambda^3-64\lambda^2\right)r^2-360\lambda^6+\left(-120\lambda^4+1320\lambda^5\right)r\end{array}\right), \tag{58}$$

where r is an independent variable. K can be derived from Equation 58. There are multiple roots for Equation 58; however, merely the real and negative roots are of physical meaning. For instance, assuming $\lambda = 1/3$, Equation (58) gives the following roots for K^2:

$$K_1^2=\frac{1}{NaNv^3}\left(\frac{1}{270}\left(71092+405\sqrt{30815}\right)^{\frac{1}{3}}-\frac{71}{270\left(71092+405\sqrt{30815}\right)^{\frac{1}{3}}}+\frac{73}{270}\right), \tag{59a}$$

$$K_2^2=\frac{1}{NaNv^3}\left[\begin{array}{l}\left(-\frac{1}{540}\left(71092+405\sqrt{30815}\right)^{\frac{1}{3}}+\frac{71}{540\left(71092+405\sqrt{30815}\right)^{\frac{1}{3}}}+\frac{73}{270}\right)\\+\frac{\sqrt{3}}{2}I\left(\frac{1}{270}\left(71092+405\sqrt{30815}\right)^{\frac{1}{3}}+\frac{71}{270\left(71092+405\sqrt{30815}\right)^{\frac{1}{3}}}\right)\end{array}\right], \tag{59b}$$

$$K_3^2=\frac{1}{NaNv^3}\left[\begin{array}{l}\left(-\frac{1}{540}\left(71092+405\sqrt{30815}\right)^{\frac{1}{3}}+\frac{71}{540\left(71092+405\sqrt{30815}\right)^{\frac{1}{3}}}+\frac{73}{270}\right)\\-\frac{\sqrt{3}}{2}I\left(\frac{1}{270}\left(71092+405\sqrt{30815}\right)^{\frac{1}{3}}+\frac{71}{270\left(71092+405\sqrt{30815}\right)^{\frac{1}{3}}}\right)\end{array}\right]. \tag{59c}$$

Two of these three roosts are not real, and hence, they can be discarded. The remaining root is real, which can be expressed as

$$K=\pm\frac{1}{\sqrt{NaNv^3}}\left(\frac{1}{270}\left(71092+405\sqrt{30815}\right)^{\frac{1}{3}}-\frac{71}{270\left(71092+405\sqrt{30815}\right)^{\frac{1}{3}}}+\frac{73}{270}\right)^{\frac{1}{2}}=\pm\frac{0.677}{\sqrt{NaNv^3}}. \tag{60}$$

Finally, the negative real root is acceptable, which can be expressed by

$$K=-\frac{0.677}{\sqrt{NaNv^3}}. \tag{61}$$

It is worth mentioning that obtaining K indeed is equal to obtaining $\theta'(0)$ as they are related together directly through Equation 17 as follows:

$$\theta'(0)=NvK. \tag{62}$$

Thus, in this particular case, that is, $\lambda = 1$, Numerical analysis of unsteady is obtained as

$$\theta'(0)=-\frac{0.677}{\sqrt{NaNv}}, \tag{63}$$

and consequently, the reduced Nusselt number (*Nur*), which is the main parameter of interest, can be calculated using Equation 13 as $Nur = -(k_{eff,hnf}/k_{eff,f})\theta'(0)$ where $(k_{eff,hnf}/k_{eff,f})$ is the conduction ratio, which comes from the thermophysical properties and hence is known.

Now, the obtained value of K can be substituted in Equation 27 to result in the complete form of the streamline boundary layer profile. Consequently, the velocity profiles can be derived by differentiation from Equation 27 with respect to η. The temperature boundary layer profile can also be achieved by utilizing Equation 17. Therefore, the accurate approximate solution of the natural convection boundary layer flow and heat transfer of hybrid nanofluids over a flat plate is obtained. It should be noticed that the obtained solution is also valid for the case of pure fluid by simply setting $Nv = Na = 1$.

4 | VALIDATION OF THE SOLUTION

The system of Equations 8 and 9 subject to the boundary conditions, Equations 10a and 10b, is analytically solved by a combination of transformation method, power series, and Padé approximation. Assuming $Nv = Na = 1$, the present study reduces to the case of a pure fluid, which was numerically studied by Cheng and Minkowycz.[9] In this case, the values of $-\theta'(0)$ are evaluated using Equations 58 and 17 for different values of λ. A comparison between the results of the present study and those reported by Cheng and Minkowycz[9] is performed in Table 3. The results of Table 3 indicate that the obtained analytical results are in excellent agreement with the numerical results of Cheng and Minkowycz.[9]

A comparison between the nondimensional temperature boundary layer profile obtained in the present study by Padé (4, 4), the numerical solution of Cheng and Minkowycz,[9] and the available experimental results[44] are depicted in Figure 2. As seen, there is an excellent agreement between the analytical, numerical, and experimental results.

In the case of isothermal wall temperature and a pure fluid, that is, $\lambda = 0$ and $Nv = Na = 1$, the temperatures boundary layer profile, accomplished using Padé (2, 2), Padé (4, 4), series size of (16), that is, $O(x^{17})$, series size of (22), and the numerical results reported by Cheng and Minkowycz[9] are depicted in Figure 3. The corresponding Padé series of (2, 2) and (4, 4) are as follows: The results show that a series solution, as well as the series-Padé (2, 2), do not follow the numerical results and diverge at $\eta = 2.5$. The value of K is calculated using Equation 58. The results indicate that the series solution with many terms ($O(x^{22})$) cannot reach the physical infinity, and it diverges. Therefore, it is clear that it was not possible to directly utilize the obtained series solution to evaluate the undetermined coefficient of K. The results of this figure show that the Padé (4, 4) follows the dimensionless temperatures profiles with high accuracy. The corresponding Padé approximations (2, 2) and (4, 4) when $\lambda = 0$ are summarized as follows:

$$\theta_{2,2}(\eta) = \frac{1 - 0.3370188880\eta + 0.03285256407\eta^2}{1 + .1123396293\eta + 0.08333333333\eta^2}, \tag{64}$$

$$\theta_{4,4}(\eta) = \frac{\begin{pmatrix} 1 + .6024637366\eta + 0.03119804175\eta^2 - 0.07406710542\eta^3 \\ + 0.009442556106\eta^4 \end{pmatrix}}{\begin{pmatrix} 1 + 1.051822254\eta + 0.5038433302\eta^2 + 0.1148926433\eta^3 \\ + 0.02589016734\eta^4 \end{pmatrix}}. \tag{65}$$

TABLE 3 A comparison between the evaluated results of $-\theta'(0)$ and the work of Cheng and Minkowycz[9] for a pure fluid when $Nv = Na = 1$

λ	Present method	Numerical[2]
0	0.4493	0.444
1/4	0.6258	0.630
1/3	0.6772	0.678
1/2	0.7701	0.761
3/4	0.8923	0.892
1	1	1.001

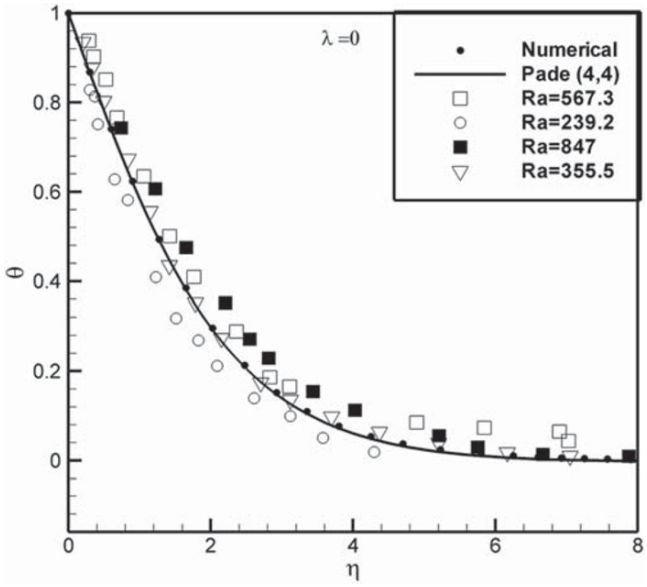

FIGURE 2 Comparison between experimental data, transformation-series Padé (4, 4), and numerical method

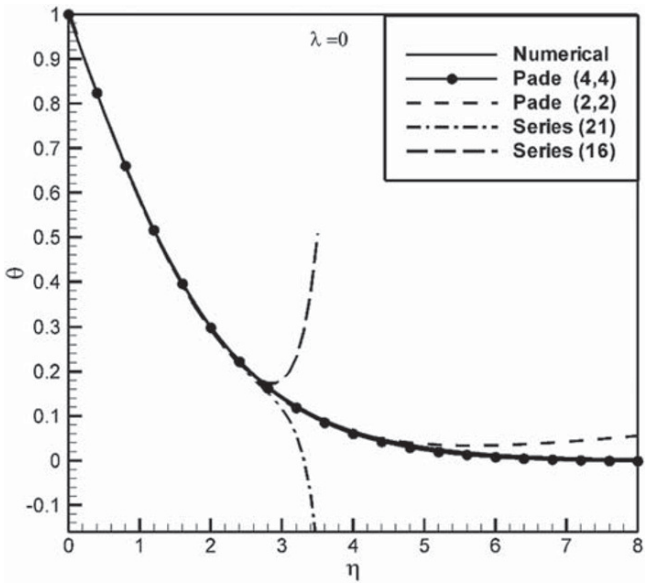

FIGURE 3 Comparison between transformation-series solution method with sizes of (15) and (20), transformation-series-Padé with sizes of (2, 2) and (4, 4), and the numerical results for the boundary layer temperature profiles

Figure 3 shows that the power series without using Padé approximants cannot follow the solution in the entire domain of the solution, and they diverge before reaching the asymptotic solution. Figure 3 indicates that the series in the form of Padé with the size of (2, 2) follows the solution but its accuracy is not good; the series solution in the form of Padé (4, 4) follows the solution with excellent precision and is almost identical with the accurate numerical solution of the problem. Therefore, the Padé approximants with the size of (4, 4) associated with evaluated K from Equation 58 is adequate for the study of the boundary layer flow and heat transfer of hybrid nanofluids.

5 | RESULTS AND DISCUSSION

Figure 4 shows the boundary layer temperature profiles for different values of the number of thermal diffusivities (Na) parameter. This figure shows that an increase in the number of thermal diffusivity increases the thickness of the thermal boundary layer. Indeed, as the thermal diffusivity of the hybrid nanofluid increases, the heat can more contently penetrate from a layer to its adjacent layer by conduction mechanism. Therefore, the increase in the number of thermal diffusivity increases the temperature in the boundary layer.

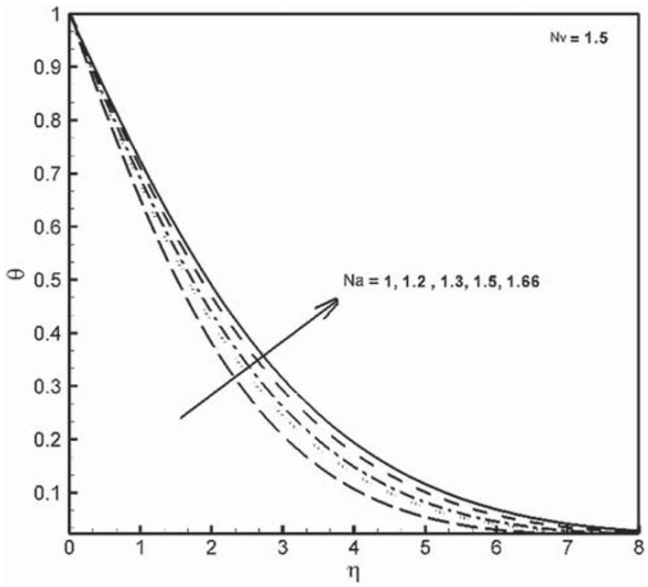

FIGURE 4 The dimensionless temperature profiles for different values of *Na*

Figure 5 depicts the nondimensional temperature profiles for selected values of the viscosity number (*Nv*). As seen, the increase of the viscosity number also increases the thickness of the thermal boundary layers. Indeed, the increase of the dynamic viscosity of hybrid nanofluid tends to reduce the velocity of the hybrid nanofluid over the plate. Any reduction of the velocity in the boundary layer reduces the heat transfer by the convective terms and hence increases the temperature in the boundary layer.

It should be noticed that the increase of *Nv*, which decrease of the magnitude of $|-\theta'(0)|$, merely results in the deterioration of the heat transfer rate from the plate. However, the increase of the thermal diffusivity number, *Na*, induces two opposite effects on the heat transfer rate from the wall. By the increase of the thickness of the boundary layer (i.e., a decrease of the magnitude of $|-\theta''(0)|$), it tends to reduce the magnitude of the reduced Nusselt number and consequently the heat transfer rate from the plate. In contrast, the increase of the thermal diffusivity parameter may increase the thermal conductivity ratio ($k_{eff}/k_{eff,f}$), which directly tends to increase the reduced Nusselt number.

In most practical cases, the increase of the thermal conductivity ratio is significant, and hence, the heat transfer rate by using hybrid nanofluids increases. However, the results of the present study indicate that in some cases in which the values of *Nv* are large, the thickness of the thermal boundary layer can significantly increase, and hence, the corresponding reduced Nusselt number may decrease, which leads to the deterioration of heat transfer. The reduced Nusselt number can be evaluated easily using Equations 13 and 58. Therefore, the present analytical solution is crucial

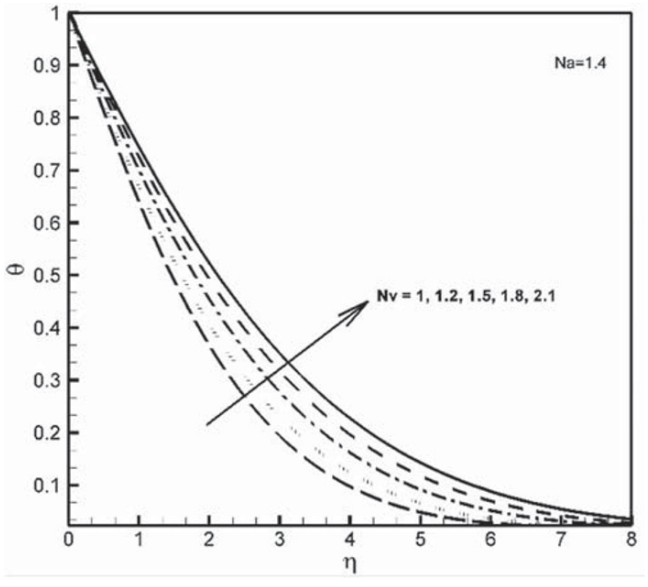

FIGURE 5 The dimensionless temperature profiles for different values of *Nv*

TABLE 4 The thermophysical properties of MWCNT–Fe_3O_4/water and computed corresponding values of *Nc* and *Nv* at the working temperature of 40°C

Volume fraction (%)	*Na*	*Nv*	*Nur*
$\varphi = 0.0$	1	1	0.667
$\varphi = 0.1$	0.8857	1.1180	0.6567
$\varphi = 0.3$	0.8392	1.3829	0.6037

in the design of heat transfer systems and choosing the appropriate types of hybrid nanofluids and nanoparticles to contently enhance the heat transfer rate from the plate without going through costly numerical procedures.

Using the data of Table 1 and Equation 63, the values of *Nur* for MWCNT–Fe_3O_4/water are computed and reported in Table 4. The values of the reduced Nusselt number (*Nur*) represent the heat transfer rate over the surface. For the case of MWCNT–Fe_3O_4/water in the glass ball porous matrix, the results of Table 4 show that using the hybrid nanoparticles reduces the heat transfer rate. This is due to the significant increase in dynamic viscosity due to the presence of MWCNTs.

6 | CONCLUSIONS

The natural convection of hybrid nanofluids over a vertical flat plate embedded in a porous medium filled with a hybrid nanofluid is theoretically analyzed. A new analytical solution based on the symbolic power series and Padé approximants is proposed. The power series solution includes an undetermined coefficient, which should be determined using the asymptotic boundary condition. A transformation method is utilized to deal with the asymptotic boundary condition and determined the undetermined coefficient analytically. The results are compared with the numerical and experimental results available in the literature in the case of pure fluid and found in the excellence agreement.

The study of hybrid nanofluids shows that the increase of the thermal diffusivity number and the viscosity number increases the thickness of the thermal boundary layer. Therefore, there are cases in which the presence of nanoparticles may deteriorate the heat transfer rate from the plate. The analytical results of the present study are crucial in engineering design and selection of appropriate nanofluids to sufficiently enhance the heat transfer rate without using time-consuming numerical procedures.

CONFLICTS OF INTEREST

This work does not have any conflicts of interest.

NOMENCLATURE

A amplitude of wall heating (K/m^{λ})
C_p specific heat at constant pressure (J/kg K)
e dummy parameter
f dimensionless stream function, dummy parameters
g gravitational acceleration (m/s^2)
h convective heat transfer coefficient (W/K)
i dummy parameter
k thermal conductivity (W/m K)
L height of the plate
Na the number of thermal diffusivity
Nur reduced Nusselt number
Nu_x local Nusselt number
Nv the number of viscosity
p pressure (Pa)
q'' surface heat flux (W/m^2)

Ra_x Rayleigh number
T fluid temperature (K)
T_∞ ambient temperature (K)
T_w surface temperature (K)
u, v Darcy velocities (m/s)
$\bar{q}'$ the total heat transfer rate through the plate of height L
x, y Cartesian coordinates (m)
X,Y dummy functions

Greek symbol

α thermal diffusivity (m^2/s)
β thermal expansion (1/K)
ε porosity
η similarity variable
θ dimensionless temperature
κ permeability (m^2)
λ prescribed the power of temperature variation
μ dynamic viscosity (kg/m s)
ρ density (kg/m^3)
ϕ nanoparticles volume fraction
ψ stream function (m^2/s)

Subscripts

eff effective value for porous medium and fluid
∞ ambient condition
f base fluid
m porous media
hnf hybrid nanofluid
p particle
1 the first type of solid nanoparticles
2 the second type of solid nanoparticles

Superscript

′ differentiation with respect to η

ORCID

Mehdi Ghalambaz https://orcid.org/0000-0001-8762-5510

REFERENCES

1. Özerinç S, Kakaç S, Yazıcıoğlu A. Enhanced thermal conductivity of nanofluids: a state-of-the-art review. *Microfluid Nanofluid*. 2010; 8(2):145-170.
2. Khanafer K, Vafai K. A critical synthesis of thermophysical characteristics of nanofluids. *Int J Heat Mass Transfer*. 2011;54(19–20):4410-4428.
3. Sundar LS, Sharma KV, Naik MT, Singh MK. Empirical and theoretical correlations on viscosity of nanofluids: a review. *Renew Sustain Energy Rev*. 2013;25:670-686.
4. Ma Y, Mohebbi R, Rashidi M, Yang Z, Sheremet M. Nanoliquid thermal convection in I-shaped multiple-pipe heat exchanger under magnetic field influence. *Physica a: Stat Mech Appl*. 2020;124028.
5. Bondareva NS, Sheremet MA. Effect of Nano-sized heat transfer enhancers on PCM-based heat sink performance at various heat loads. *Nanomaterials*. 2020;10(1):1-17.
6. Wu S, Zhu D, Li X, Li H, Lei J. Thermal energy storage behavior of Al_2O_3–H_2O nanofluids. *Thermochim Acta*. 2009;483:73-77.

7. Saidur R, Leong KY, Mohammad HA. A review on applications and challenges of nanofluids. *Renew Sustain Energy Rev*. 2011;15:1646-1668.
8. Gorla RRS, Chamkha AJ, Rashad AM. Mixed convective boundary layer flow over a vertical wedge embedded in a porous medium saturated with a nanofluid: natural convection dominated regime. *Nanoscale Res Lett*. 2011;6(1):55-66.
9. Cheng P, Minkowycz WJ. Free convection about a vertical flat plate embedded in a porous medium with application to heat transfer from a dike. *J Geophys Res*. 1977;82:2040-2044.
10. Belhachmi Z, Brighi B, Sac-Epee JM, Taous K. Numerical simulations of free convection about a vertical flat plate embedded in a porous medium. *Comput Geosci*. 2003;7:137-166.
11. Chamkha AJ, Al-Mudhaf A, Al-Yatama J. Double-diffusive convective flow of a micropolar fluid over a vertical plate embedded in a porous medium with a chemical reaction. *Int J Fluid Mech Res*. 2004;31:529-551.
12. Takhar HS, Chamkha AJ, Gorla RSR. Combined convection-radiation interaction along a vertical flat plate in a porous medium. *Int J Fluid Mech Res*. 2005;32:139-156.
13. Chamkha AJ, Al-Mudhaf AF, Pop I. Effect of heat generation or absorption on thermophoretic free convection boundary layer from a vertical flat plate embedded in a porous medium. *Int Commun Heat Mass Transfer*. 2006;33(9):1096-1102.
14. Gorla RSR, Chamkha AJ, Takhar HS. Mixed convection in non-Newtonian fluids along a vertical plate in porous media with constant surface heat flux. *Thermal Energy Power Eng*. 2013;2:66-71.
15. Ahmed S, Batin A, Chamkha J. A finite difference approach in porous media transport modeling for magnetohydrodynamic unsteady flow over a vertical plate. *Int J Num Methods Heat Fluid Flow*. 2014;24(5):1204-1223.
16. Chamkha AJ, Aly AM, Mansour MA. Unsteady natural convective power-law fluid flow past a vertical plate embedded in a non-Darcian porous medium in the presence of a homogeneous chemical reaction. *Nonlinear Anal: Model Control*. 2010;15:139-154.
17. Patil PM, Chamkha AJ. Heat and mass transfer from mixed convection flow of polar fluid along a plate in porous media with chemical reaction. *Int J Num Methods Heat Fluid Flow*. 2013;23(5):899-926.
18. Ghalambaz M, Groşan T, Pop I. Mixed convection boundary layer flow and heat transfer over a vertical plate embedded in a porous medium filled with a suspension of nano-encapsulated phase change materials. *J Mol Liq*. 2019;293:111432.
19. Xu H. An explicit analytic solution for free convection about a vertical flat plate embedded in a porous medium by means of homotopy analysis method. *Appl Math Comput*. 2004;2:433-443.
20. Chamkha AJ, Quadri MMA. Simultaneous heat and mass transfer by natural convection from a plate embedded in a porous medium with thermal dispersion effects. *Heat Mass Transfer*. 2003;39(7):561-569.
21. Chandrasekar M, Suresh S. A review on the mechanisms of heat transport in Nanofluids. *Heat Transfer Eng*. 2009;30(14):1136-1150.
22. Kleinstreuer C, Feng Y. Experimental and theoretical studies of nanofluid thermal conductivity enhancement: a review. *Nanoscale Res Lett*. 2011;6(1):229.
23. Mahian O, Kolsi L, Amani M, et al. Recent advances in modeling and simulation of nanofluid flows-part I: fundamentals and theory. *Phys Rep*. 2019;790:1-48.
24. Ahmadi MH, Ahmadi MA, Nazari MA, Mahian O, Ghasempour R. A proposed model to predict thermal conductivity ratio of Al_2O_3/EG nanofluid by applying least squares support vector machine (LSSVM) and genetic algorithm as a connectionist approach. *J Therm Anal Calorim*. 2019;135(1):271-281.
25. Sheikholeslami M, Sheremet MA, Shafee A, Tlili I. Simulation of nanoliquid thermogravitational convection within a porous chamber imposing magnetic and radiation impacts. *Physica A*. 2020;124058.
26. Babu JR, Kumar KK, Rao SS. State-of-art review on hybrid nanofluids. *Renew Sustain Energy Rev*. 2017;77:551-565.
27. Mehryan S, Sheremet MA, Soltani M, Izadi M. Natural convection of magnetic hybrid nanofluid inside a double-porous medium using two-equation energy model. *J Mol Liq*. 2019;277:959-970.
28. Ghalambaz M, Sheremet MA, Mehryan S, Kashkooli FM, Pop I. Local thermal non-equilibrium analysis of conjugate free convection within a porous enclosure occupied with Ag–MgO hybrid nanofluid. *J Therm Anal Calorim*. 2019;135(2):1381-1398.
29. Izadi M, Mohebbi R, Karimi D, Sheremet MA. Numerical simulation of natural convection heat transfer inside a? shaped cavity filled by a MWCNT-Fe3O4/water hybrid nanofluids using LBM. *Chem Eng Process-Process Intensif*. 2018;125:56-66.
30. Chamkha AJ, Miroshnichenko IV, Sheremet MA. Numerical analysis of unsteady conjugate natural convection of hybrid water-based nanofluid in a semicircular cavity. *J Therm Sci Eng Appl*. 2017;9(4):041004.
31. Mohebbi R, Mehryan S, Izadi M, Mahian O. Natural convection of hybrid nanofluids inside a partitioned porous cavity for application in solar power plants. *J Therm Anal Calorim*. 2019;137(5):1719-1733.
32. Rashidi I, Kolsi L, Ahmadi G, Mahian O, Wongwises S, Abu-Nada E. Three-dimensional modelling of natural convection and entropy generation in a vertical cylinder under heterogeneous heat flux using nanofluids. *Int J Num Methods Heat Fluid Flow*. 2019;30(1):119-142.
33. Hajjar A, Mehryan S, Ghalambaz M. Time periodic natural convection heat transfer in a nano-encapsulated phase-change suspension. *Int J Mech Sci*. 2020;166:105243.
34. Ghalambaz M, Mehryan S, Hajjar A, Veisimoradi A. Unsteady natural convection flow of a suspension comprising Nano-encapsulated phase change materials (NEPCMs) in a porous medium. *Adv Powder Technol*. 2019;30(1):954-966.
35. Mehryan S, Ghalambaz M, Gargari LS, Hajjar A, Sheremet M. Natural convection flow of a suspension containing nano-encapsulated phase change particles in an eccentric annulus. *J Energy Storage*. 2020;28:101236.
36. Nield DA, Bejan A. *Convection in Porous Media*. Third Edition ed. New York: Springer; 2013.

37. Sundar LS, Sharma K, Singh MK, Sousa A. Hybrid nanofluids preparation, thermal properties, heat transfer and friction factor—a review. *Renew Sustain Energy Rev*. 2017;68:185-198.
38. Sundar LS, Singh MK, Sousa AC. Enhanced heat transfer and friction factor of MWCNT–Fe3O4/water hybrid nanofluids. *Int CommunHeat Mass Transfer*. 2014;52:73-83.
39. Ghalambaz M, Sheremet MA, Pop I. Free convection in a parallelogrammic porous cavity filled with a nanofluid using Tiwari and Das' nanofluid model. *PLoS One*. 2015;10(5):e0126486.
40. Guzel N, Bayram M. On the numerical solution of stiff systems. *Appl Math Comput*. 2005;170:230-236.
41. Celik E, Bayram M. Arbitrary order numerical method for solving differential-algebraic equation by Padé series. *Appl Math Comput*. 2003;137:57-65.
42. Simsek H, Celik E. The successive approximation method and Padé approximants for solutions the non-linear boundary value problem. *Appl Math Comput*. 2003;146(2–3):681-690.
43. Wazwaz AM. Analytical approximations and Padé approximants for Volterra's population mode. *Appl Math Comput*. 1999;100:13-25.
44. Evans GH, Plumb OA, editors. Natural convection from a vertical isothermal surface imbedded in a saturated porous medium. AIAA-ASME Thermophysics and Heat Transfer Conf; 1978; Palo Alto California.

How to cite this article: Ghalambaz M, Noghrehabadi A, Chamkha A, Nadeem S. Analytical solution of free convection heat transfer of hybrid nanofluids over a vertical flat plate embedded in a porous medium. *Math Meth Appl Sci*. 2020;1–19. https://doi.org/10.1002/mma.6457